

Original Article

Sediment sources and their impacts on a check dam-controlled watershed, Loess Plateau, China

BAI Lu-lu¹  <https://orcid.org/0000-0003-0268-0858>; e-mail: bailulu222@163.com
SHI Peng^{1,2*}  <https://orcid.org/0000-0002-5802-8386>;  e-mail: shipeng015@163.com
WANG Wen^{1,2}  <https://orcid.org/0009-0005-1324-4850>; e-mail: 1683542070@qq.com
LI Zhan-bin^{1,2}  <https://orcid.org/0000-0001-5341-1194>; e-mail: zqli@xaut.edu.cn
YU Kun-xia^{1,2}  <https://orcid.org/0000-0001-5521-7387>; e-mail: yukunxia@126.com
LI Peng^{1,2}  <https://orcid.org/0000-0003-1795-6466>; e-mail: lipeng74@163.com
CUI Ling-zhou^{3*}  <https://orcid.org/0000-0002-2266-3046>;  e-mail: clingzhou@126.com
SHEN Rong-jian⁴  <https://orcid.org/0009-0007-6532-1963>; e-mail: syj600502@163.com
GUAN Mu-hong⁴  <https://orcid.org/0009-0000-5649-6189>; e-mail: gmh600502@163.com
DU Xin-chun⁴  <https://orcid.org/0009-0000-3394-3249>; e-mail: dxc600502@163.com
ZHANG Xun-le⁴  <https://orcid.org/0009-0009-4001-9308>; e-mail: zx1600502@163.com
CHEN Wen-fu⁴  <https://orcid.org/0009-0007-5071-852X>; e-mail: cwf600502@163.com

*Corresponding author

¹ State Key Laboratory of Eco-hydraulics in Northwest Arid Region of China, Xi'an University of Technology, Xi'an 710048, China

² Key Laboratory of National Forestry Administration on Ecological Hydrology and Disaster Prevention in Arid Regions, Xi'an University of Technology, Xi'an 710048, China

³ College of Life and Environmental Science, Wenzhou University, Wenzhou 325035, China

⁴ Anhui Water Resources Development Co., Ltd., Bengbu 233010, China

Citation: Bai LL, Shi P, Wang W, et al. (2023) Sediment sources and their impacts on a check dam-controlled watershed, Loess Plateau, China. Journal of Mountain Science 20(6). <https://doi.org/10.1007/s11629-022-7888-2>

© Science Press, Institute of Mountain Hazards and Environment, CAS and Springer-Verlag GmbH Germany, part of Springer Nature 2023

Abstract: Soil erosion is a major issue in Loess Plateau, China, and quantitative analyses of sediment sources are crucial for soil erosion control. In this study, a combination of flood couplet analysis and composite fingerprint identification was used for historical reconstructions of soil erosion in sediment source areas in Loess Plateau. Each flood couplet was

constructed based on sediment ¹³⁷Cs activity, and past soil erosion was calculated using soil bulk density and storage capacity curves. The contribution rates of the sediment sources were calculated using the fingerprinting method, and the amount of erosion in the sediment source areas was estimated. The best fingerprint combination (Cr, Ni, V, and TOC) enabled a 97.2% recognition of sediment sources from 29 flood events (1956–1990) in the Loess Plateau. The

Received: 29-Dec-2022

Revised: 19-Apr-2023

Accepted: 21-May-2023

contribution rates of gullies, farmland, grassland, and shrubland were 44.89%, 26.38%, 10.49%, and 18.24%, respectively. These four land use types contributed 1,227, 751, 512, and 279 tons of sediments, respectively. Re-vegetation decreased soil erosion (1966–1983), whereas deforestation increased soil erosion (1956–1965 and 1984–1990). Rational soil and water conservation measures on slopes and check dam construction in gullies are therefore suggested to mitigate erosion.

Keywords: Check dam; Sediment source; Soil and water conservation; Land use changes; Loess Plateau

1 Introduction

Soil and water losses are serious issues on the Loess Plateau, mainly because of the complex hydrogeological environment and land degradation caused by unreasonable land use (Wen and Zhen 2020; Shi et al. 2021; Xiao et al. 2022). The total soil erosion area accounts for approximately 61% of the Loess Plateau (Wen and Deng 2020). Although the average soil erosion modulus in this region is 5000 t $\text{km}^{-2} \text{a}^{-1}$, it reaches 2.0×10^4 – 3.0×10^4 t $\text{km}^{-2} \text{a}^{-1}$ in some areas (Chen et al. 2007; Wang et al. 2021). Soil erosion causes problems (Poesen 2017) by decreasing soil fertility and continuously decreasing the available arable land area (Gholami et al. 2021). Sediment movement combined with heavy metal pollution of rivers and lakes also leads to eutrophication of water bodies (Fielding et al. 2020). In addition, mudslides and floods are more likely to occur in eroded areas under rainstorm conditions, posing major threats to human life and property (Gao and Sang 2017). To address these problems, reasonable soil and water conservation measures at the watershed scale are needed. Optimizing these measures is essential for quantitatively calculating the contribution rates of sediment sources at the watershed scale (Hu et al. 2020; Mekonnen 2021).

Traditional sediment source identification methods include runoff plot observation (Poesen and Hooke 1997; Poesen et al. 2003), runoff and sediment data analysis (Nistor and Michael 2005; Cavalli et al. 2013), and rare earth elemental tracers (Silva-Filho et al. 2010; Jia et al. 2014), all of which have certain limitations. The accuracy of the runoff plot observation method is low, rendering it unsuitable for large-scale research. It is also difficult to obtain data

for runoff and sediment data analysis; therefore, this method cannot be used without a hydrological station in a certain watershed. The experimental cost and workload used in the rare earth elemental tracer method are high, rendering it suitable only for runoff plot scale. Its application is therefore limited at large spatial scales and for large sediment source areas. Compared with these methods, the fingerprinting method uses the physical, chemical, biological, and optical properties of the soil as fingerprint tracers, and does not discuss complex sediment production and transport processes, thereby providing a new method for sediment source research (Walling et al. 1979; Lance et al. 1986). The single fingerprinting method has a limited ability to discriminate sediment sources from multiple sources (≥ 3) and has certain uncertainties (Collins et al. 1998; Collins et al. 2010; Boudreault et al. 2019; Niu et al. 2019). The composite fingerprinting method uses multiple tracers to improve the credibility of the sediment source identification (Collins et al. 2010; Evrard et al. 2019). Therefore, composite fingerprint identification technology is a reliable method for investigating the origin of sediments, and has been widely used for lake reservoirs (Slimane et al. 2013; Palazón et al. 2015), water erosion crisscross areas (Ahmady-Birgani et al. 2018; Gaspar et al. 2019), check dam-controlled watersheds (Chen et al. 2016a), and other sedimentary environments (Muñoz-Arcos et al. 2021).

The soil erosion problems on the Loess Plateau have been acknowledged since the 1950s. During the past 70 years, the Chinese government has introduced a series of policies to control serious soil and water losses (Lin and Yao 2014; Feng et al. 2016; Cheng et al. 2018; Wen and Zhen 2020; Fig. 1). These conservation measures can be divided into two categories: re-vegetation and engineering measures (Wen and Deng 2020). By 2018, soil and water conservation on the Loess Plateau had greatly improved: forest and grass coverage increased to 63% from 20% in the 1980s, terraced area increased from $1.4 \times 10^4 \text{ km}^2$ to $5.5 \times 10^4 \text{ km}^2$, and more than 59,000 check dams were built (Feng et al. 2016; Xu et al. 2018; Hu and Zhang 2020). Large-scale ecological reconstruction has effectively controlled soil erosion on the Loess Plateau (Hu and Zhang 2020; Wen and Zhen 2020).

Check dams are efficient ditch engineering measures that not only have substantial effects on soil and water conservation, but also retain most of the

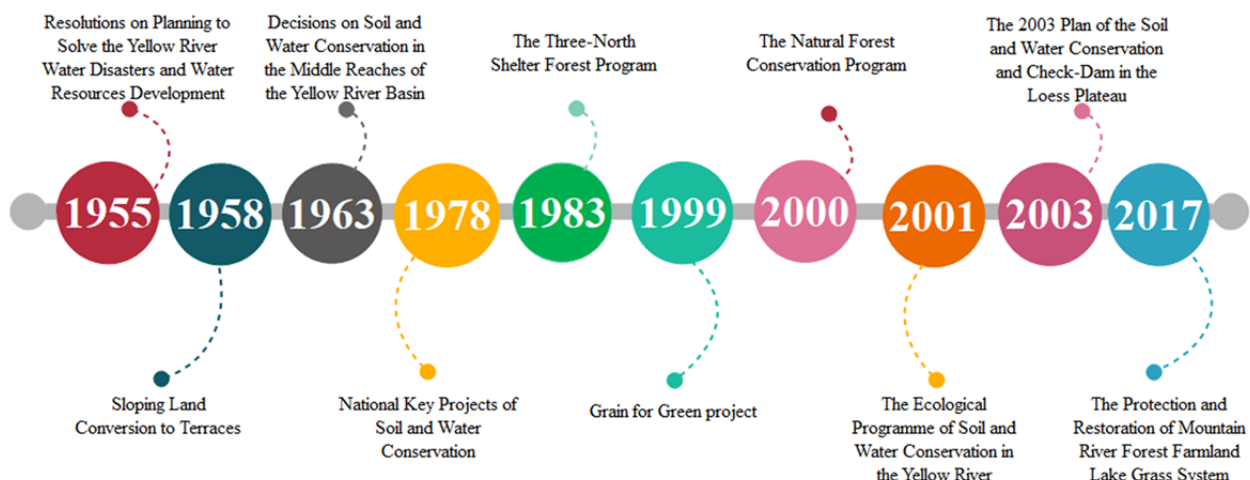


Fig. 1 Development history of policies and plans for main soil and water conservation programs in the Loess Plateau.

transported sediment (Chen et al. 2019). Check dams record both natural and human behavior in their deposits, thereby providing information about sediment sources on the Loess Plateau (Zhang et al. 2020). It is crucial to determine the soil erosion rates and sediment sources in check dam-controlled watersheds on the Loess Plateau using the retained sediment. These data can be used for strategic sustainable management planning. The historical variations in sediment yield in small watersheds can be determined by analyzing the sediment intercepted by the check dams (Zhao et al. 2017). Combined with the composite fingerprinting method, the soil erosion rate(s) in the sediment source region(s) can also be calculated quantitatively. The main objectives of this study were to: (1) determine the historical sedimentary processes in a dam-controlled watershed, (2) quantify the sediment source(s) and yield(s), and (3) analyze the relationships between environmental changes and soil erosion in the source region(s).

2 Materials and Methods

2.1 Study area

The Nianyangou watershed is located in the center of the Loess Plateau region, and is a typical gully region with an area of 1.28 km^2 (Fig. 2). It is characterized by terrain cracks, steep slopes, deep ditches, and complex terrain, with an average annual erosion rate of $15,000 \text{ t km}^{-2}$. The region is characterized by a continental monsoon climate, with

an average annual temperature of 8.60°C and average annual precipitation of 513 mm. Precipitation mainly occurs in the summer (June–September), which accounts for more than 70% of the total annual precipitation. The soil in this region is mainly loess (Calcaric Regosols in the WRB soil classification, IUSS Working Group; W.R.B. 2006) with weak cohesion.

Three check dams were constructed in the Nianyangou watershed: No. 1, No. 2, and No. 3. We selected the No. 3 check dam for this study, as it does not contain a drainage structure. The dam was built in 1956 and has an area of 0.181 km^2 and an elevation of 1,027–1,188 m. The main land use types in the study area are farmland, grassland, and shrubland. The farmland is mainly used to grow wheat in the winter and corn in the spring. The main grass species found in the grassland are *liquorice*, *Artemisia giralddii*, and *Glycyrrhiza*. The shrubland mainly consists of *Caragana korshinskii* and *Hippophae rhamnoides*. Based on communication with the local farmers, check dam No. 3 was filled with silt in 1990, and the farmers claim that no water spilled over the top during dam operation. In addition, the No. 3 check dam does not have a drainage structure; thus, it can be assumed that its closure efficiency is 100% and that all sediment can be traced.

According to the local farmers, the cultivated land area in the watershed has not changed over time, whereas the grassland and shrubland have undergone natural recovery and succession. Therefore, it is believed that no significant changes in land use have occurred within the watershed. The physical and chemical properties of the sediment samples collected

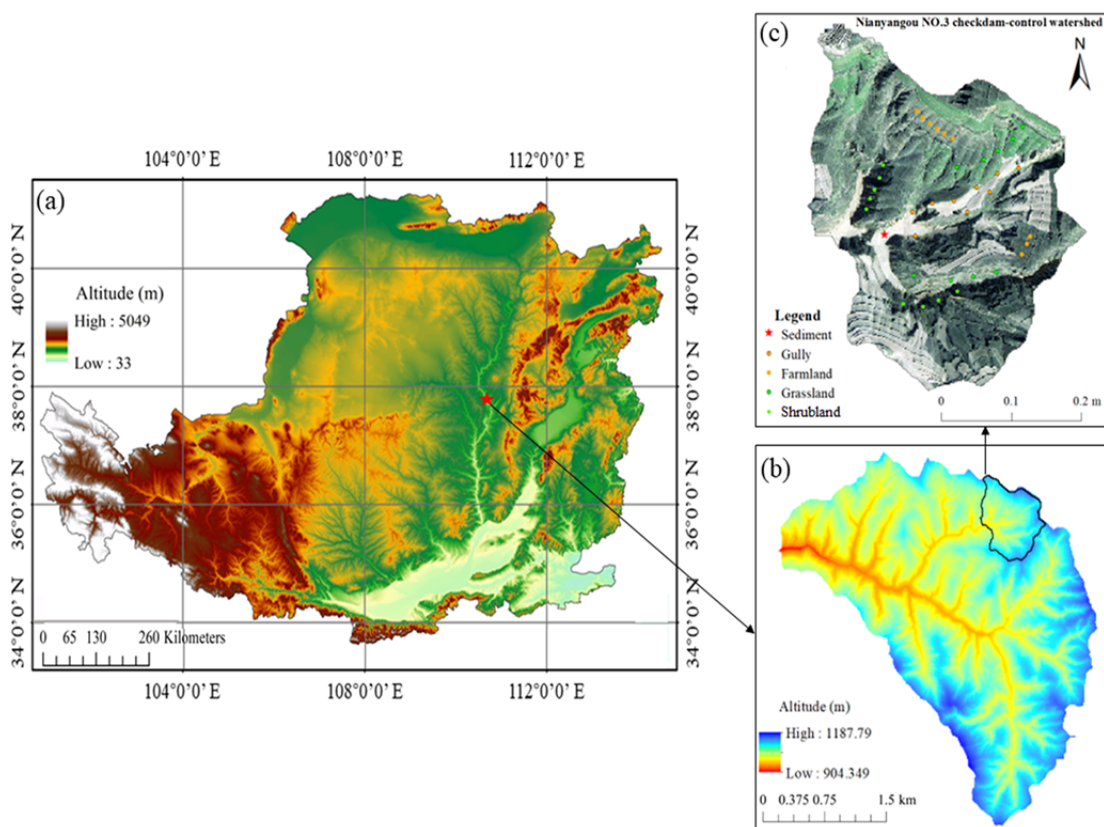


Fig. 2 Location of the study area and sampling points. (a) Location of the Loess Plateau. (b) Location of Wangmaogou watershed. (c) Location of sampling points in the Nianyangou NO.3 check dam-controlled watershed.

in this study were similar to the historical soil properties in the area. In addition, after the check dam was completely filled in 1990, the dam land was only used as cultivated land for planting and no

chemical fertilizers were used. Therefore, we inferred that the uppermost sediment layer in the sediment core (after excluding the plow layer) was deposited in 1990.

2.2 Sample collection and analysis

Sediment source samples and sediment cores were collected from the study area. Gullies, farmland, shrubland, and grassland were identified as potential sediment sources in the dam control area (Fig. 3). The topographic features (e.g., slope position, grade, and direction) of the farmland, shrubland, and grassland areas were similar (Fig. 2). In 2019, nine plots were established in each land use area. Within each plot, three sites were established at the top, middle, and bottom locations of the slope. A soil drill (70 mm diameter) was used to collect surface soil samples (0–5 cm). Soil samples from the same plot were mixed into a single sample. A total of 36 soil samples were collected from the potential source areas.

In the dam-land, a gravity sampler (mechanical drill) was used to sample the sediment. A sediment core (70 mm diameter) was collected ~30 m from the

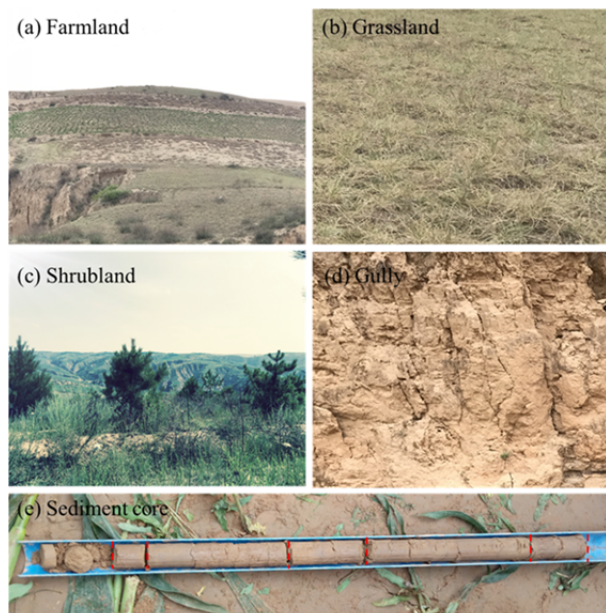


Fig. 3 Landscape of the sediment sources. (a) Farmland; (b) Grassland; (c) Shrubland; (d) Gully; (e) Sediment core.

dam body. The top layer (40 cm) of this sediment core was the cultivated layer. After removing the cultivated layer, the sediment core was 5.98 m in length. Standard sediment stratification has upper fine soil and basal coarse sand, which together form a complete layer. The boundaries of the sediment layers were clearly identified using these characteristics (Fig. 3e). Based on on-site identification, the sediment core contained 29 layers. Each layer corresponded to a specific flood event and was treated as a discrete sediment sample. The thickness of each sediment layer was measured using a steel ruler. The soil and sediment samples were transported to the laboratory for analysis.

All samples were air-dried at 25°C for 15 days, then sieved successively through 2 mm and < 63 µm sieves prior to analysis. ¹³⁷Cs activity were measured using a hyper-pure coaxial germanium detector connected to a multi-channel digital analyzer system using soil samples sieving to 2 mm (GMX50P4-83, ORTEC, USA). All soil sample weights exceeded 300 g, which were measured at 661.6 keV with a counting time greater than 28,800 s. The soil particle compositions were measured using a Master Sizer 2000 instrument (British Malvern, UK). A colorimetric method was used to measure soil total organic carbon (TOC) (multi N/C 3100, Analytik Jena AG, Jena, Germany) (Sims and Haby 1971). Soil total nitrogen (TN) and total phosphorus (TP) were quantitatively analyzed using an elemental analyzer (Clever Chem Anna, DeChem-Tech, Germany). Trace elements were extracted using microwave digestion and analyzed using inductively coupled plasma spectrometry. Arsenic (As), cobalt (Co), chromium (Cr), copper (Cu), nickel (Ni), manganese (Mn), vanadium (V), and zinc (Zn) were analyzed using inductively coupled plasma mass spectrometry (ICP-MS; Agilent 7500, Agilent Technologies, Santa Clara, CA, USA).

2.3 Sediment source analysis and sediment yield estimates

2.3.1 Obtaining an optimal combination of fingerprints

When soil physicochemical properties are used as tracers to determine the sediment sources, their non-conservative behaviors must be considered (Koiter et al. 2013). Conservative tests of tracers consist of three important tests: the range, coefficient of variation (CV

test), and Kruskal–Wallis h (H test) tests. In the range test, the tracer concentration range of the core sample must be within the range of the sediment source sample. In the CV test, the CV of the core sample tracer concentration is smaller than that of the sediment source sample. These two tests are applied to ensure conservative behavior of the tracer. A tracer that passes both tests is not lost during erosion and sediment transport. The H test confirms the ability of individual tracer properties to distinguish between sediment sources. When the *P* value of the H test for a tracer concentration is < 0.05, the tracer is better at distinguishing between sediment sources. However, the H test does not confirm the differences between all possible combinations of the source category (Koiter et al. 2013). Therefore, stepwise discriminant function analysis (DFA) was used to further evaluate the discriminant ability of tracer properties that passed all three conservative tests (Koiter et al. 2013). DFA can determine the optimal combination of tracers, as it is based on the minimization of Wilks' λ , and input/removal of a tracer from the sediment source zone reduces the variability between the tracer classes.

2.3.2 Walling mixing model for sediment sources

After obtaining the optimal set of fingerprint tracers, the Walling mixing model (Walling 2005) was used to calculate the percentage contribution of each sediment source. When using the fingerprinting method to identify sediment sources, the effects of different particle size compositions and organic matter contents between the sediment source and core samples are usually considered. In this study, the potential tracers were all measured at the same particle size (< 63 µm); thus, the use of correction tracers was not considered. Therefore, no weighting factor, organic matter, or particle size correction was applied to the Walling model in this study. Each tracer yields a linear equation relating the tracer concentrations of the core sample and the sediment source sample multiplied by an unknown contribution rate. In this study, the calculation of Eq. 1 was performed using the solver add-in program in Microsoft Excel. The boundary conditions for its solution are Eq. 2 and Eq. 3, which indicate that the contribution rates are non-negative and have a sum of 1. The goodness-of-fit (GOF) was used to characterize the relative error of the calculated result. In general, the results of the mixed model are acceptable when

the GOF is greater than 0.8 (Walling 2005).

$$R_{es} = \sum_{i=1}^n \left[\frac{C_i - \left(\sum_{s=1}^m C_{si} P_s \right)^2}{C_i} \right] \quad (1)$$

$$0 \leq P_s \leq 1 \quad (2)$$

$$\sum_{s=1}^n P_s = 1 \quad (3)$$

$$GOF = \left[1 - \frac{1}{n} \sum_{i=1}^n \frac{C_i - \sum_{s=1}^m P_s C_{si}}{C_i} \right] \times 100\% \quad (4)$$

where n is the optimal number of fingerprint tracers; C_i is the concentration of fingerprint tracer i in the core sample; P_s is the proportional contribution rate of sediment from the source sample S ; C_{si} is the average concentration of fingerprint tracer i in the sediment source area; and m is the number of sediment source areas.

2.3.3 Estimation of sediment yields

When dividing the layers in the sediment core, three soil samples were collected from each thick layer to determine the bulk density of a typical soil layer. The simulated soil bulk density curve was then obtained (Eq. 5) (Fig. 4). The silting capacity curve of the dam was provided by the local department of soil and water conservation (Fig. 5) and could be fit to Eq. 6.

$$\gamma = 0.1335 \ln(x) + 0.6971 \quad (5)$$

where γ is the soil bulk density (g cm^{-3}) and x is the soil depth (cm).

$$S = 99.84E^2 - 200405E + 100570642 \quad (6)$$

where S is the silting area (m^2) and E is the ground elevation (m).

3 Results

3.1 Establishing a flood couplet chronology

Sediment core of No.3 check dam has been continuously accumulating from 1956 to 1990 (removing the cultivated layer). During this period, a total of 29 sedimentary layers were deposited, which are closely related to the ^{137}Cs activity and particle composition of the sediment core (Fig. 6). The sediment thickness deposited after each flood varied. The thickest sedimentation was observed in the 3rd layer (33.2 cm), followed by the 24th layer (31.5 cm).

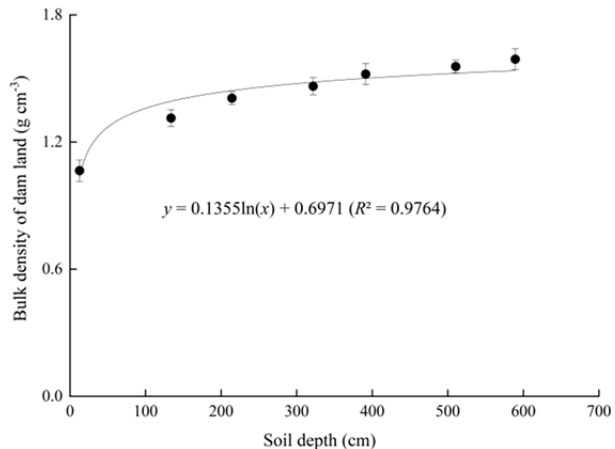


Fig.4 Simulated soil bulk density curve.

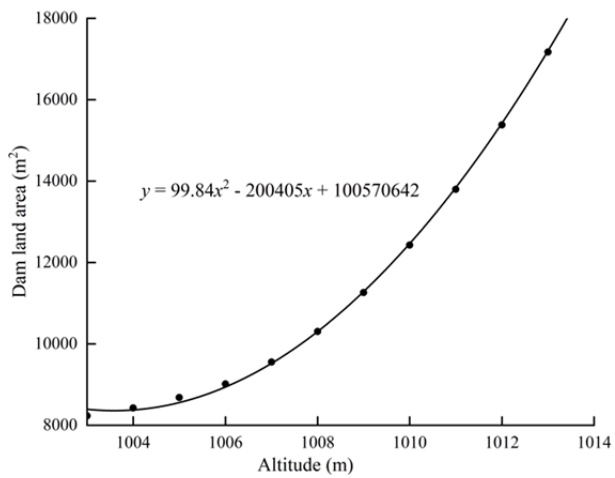


Fig.5 Simulated altitude and silt area curve of check dam.

The thinnest sedimentation was in the 6th layer (11.2 cm) (Fig. 6).

The soil particle composition of the sediment core exhibits significant variations ($P < 0.05$). Specifically, the sediment layer is mainly composed of sand particles (75.20%) and silt particles (24.53%), with minimal clay particle content (0.27%) (Fig. 6). Meanwhile, the variation coefficient of soil particle composition in different sedimentary layers had a similar order: sand (31.20%) > silt (21.25%) > clay (10.28%) (Fig. 6). The substantial difference in soil particle composition can reflect the impact of water dynamics on sediment transport and erosion in small watersheds.

Changes in the activity of ^{137}Cs can reflect the time of sediment deposition in a small watershed. The global deposition of ^{137}Cs fallout extended from the mid-1950s until the 1970s, with maximum fallout occurring in 1963 in the northern hemisphere. In the

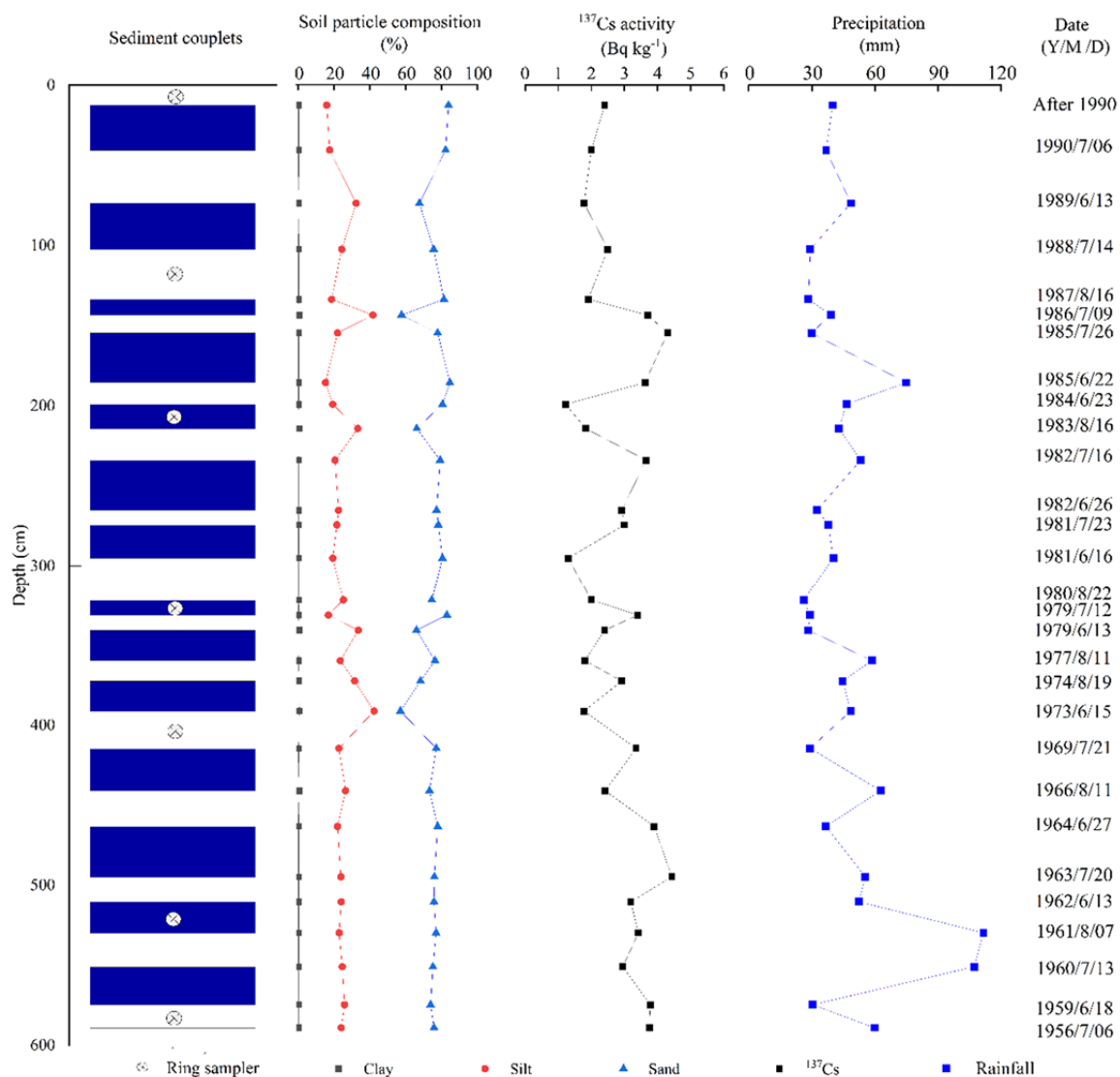


Fig.6 Distribution of sediment, soil particle composition, ^{137}Cs activities and precipitation. \otimes : It is flood couples sampled using a ring sampler for estimates of the bulk density of the sedimentation.

24th layer, there is a high peak in ^{137}Cs activity (4.68 Bq kg^{-1}) (Fig. 6), which corresponds to 1986 in the global deposition process of ^{137}Cs mentioned above. Additionally, the 7th layer has a second peak (4.27 Bq kg^{-1}) (Fig. 6), which corresponds to Chernobyl nuclear power plant in the former Soviet Union in 1986. Subsequently, the sedimentation process of No.3 check dam was reconstructed based on the flood events during that period (Fig. 6).

3.2 Sediment yields of each flood

The volumes of the flood couples in the 29 layers were calculated using the height area curve of the check dam combined with the actual elevation of the

check dam, as well as the actual thickness of the flood couplet. From 1956 to July 1990, the total sediment volume of the dam was $56,121 \text{ m}^3$. In addition, the volume of each sedimentary layer differs, with an average value of $1,935 \text{ m}^3$, and the sediment deposition shows a significant level of variation (coefficient of variation is 32.50%). Among them, the sediment volume of the 3rd layer was the largest ($3,109 \text{ m}^3$), whereas that of the 13th layer was the smallest (849 m^3).

The amount of erosion in each sedimentary cycle was estimated based on the soil bulk density curve (Fig. 7). The total amount of sediment deposited by the dam during the observation period was $\sim 80,350 \text{ t}$ and varied widely among the different layers. The amount

of each sedimentary layer differs, with an average value of 3,350 t, and the amount of them shows a significant level of variation (coefficient of variation is 39.20%). Among them, the sediment yield in the 7th layer was the highest (4,465 t), whereas that of the 13th layer was the smallest (1,230 t). In general, the sediment deposition in the dam-controlled watershed can be categorized into three erosion stages, including first stage (1956–1965), second stage (1966–1983), and third stage (1984–1990). In first stage, the sediment yield of the dam-controlled watershed is about 31,570 t, and the soil erosion modulus is 14,160 t km⁻², indicating an intense erosion stage (Fig. 7). During the second stage, the sediment yields of the dam-controlled approximately 31,070 t, and the soil erosion modulus is 9,590 t km⁻², which is relatively lower than that of the first stage (Fig. 7). In third stage, the sediment yield is about 17,710 t, and the soil erosion modulus is 13,110 t km⁻², which is relatively higher than that of the second stage (Fig. 7).

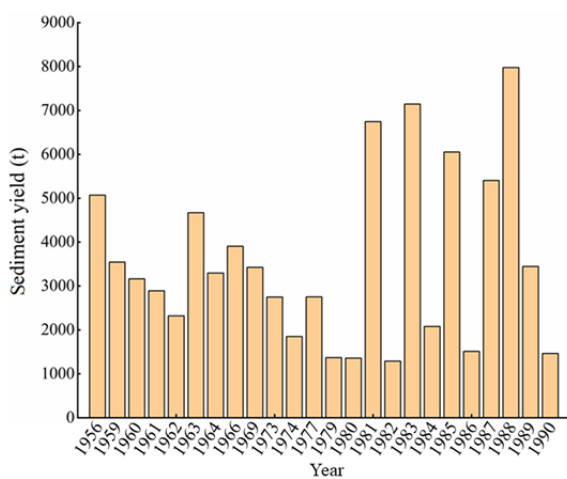


Fig. 7 Annual erosion of check dam during observation period.

3.3 Sediment source quantification

The minimum concentration of Cu in sediment is 14.51 mg kg⁻¹, while the minimum concentration of Cu in sediment source is 15.86 mg kg⁻¹ (Table 1). Therefore, Cu cannot satisfy the mean limit and is removed. For ¹³⁷Cs, its coefficient of variation in sediment (0.34) was greater than its coefficient of variation in source samples (0.31) (Table 1), so it could not meet the coefficient of variation condition and was removed. Similarly, Clay and silt indicators were also removed. Based on the results of K-W test, no significant differences were removed, including

Mn, Co, As and Sb (Table 1). In geochemical tracers, V, Cr, Ni, Zn, TOC, and Sand were obtained by the range restriction condition, mean limit condition, and K-W test (Table 1, Fig. 8). DFA was used to distinguish between the different sediment sources (Fig. 9). The optimal combination of heavy metals (Cr, Ni, and V) and TOC was then obtained. The total identification rate using these tracers was 97.2% (Table 2). The contribution rates of the four sediment sources were: gullies (44.89%) > farmland (26.38%) > shrubland (18.24%) > grassland (10.49%) (Fig. 10).

In the 29 rainfall events, the average sediment yield from gullies was 1,227 t, and that from farmland was 751 t. Shrubland and grassland contributed average sediment yields of 512 and 279 t, respectively (Fig. 11). The largest sediment yield from the gullies was in the 12th layer (~ 2,435 t). The largest sediment yield from farmland was in the 15th layer (~ 1,559 t). The largest sediment yields from grassland (676 t) and shrubland (960 t) were in the 24th and 3rd layers, respectively (Fig. 11). Overall, the sedimentation process of the dam-controlled watershed can be divided into three erosion stages, including intense erosion, gentle stage, and relatively intense erosion.

4 Discussion

4.1 Sediment yields reflect soil erosion from the slope

Based on the composite fingerprint tracing and flood couplet analyses, the sediment sources and yields in the source area of the No. 3 dam (Nianyangou Basin) from 1956–1990 were quantitatively analyzed. The results provide valuable evidence for historical studies of erosion and sediment yields in the source areas of the watershed. The sediment yields, annual rainfall, and annual rainfall erosivity varied by source area (Fig. 11). The data also emphasize the annual variations in sediment yield and peak sediment yield during the operation of the check dam. In general, the sediment yields of the gully walls, cultivated land, and grassland decreased over time, whereas the sediment yield of the shrubland did not change substantial. Zhang et al. (2020) also used this technique to calculate sediment source yields in the Laoyeman catchment, and found that gullies were the main source area (9.8–80.1%). Zhang et al. (2017) used an optimal fingerprint

Table 1 Descriptive statistics of tracer properties of potential sediment sources and sedimentary sediments and Kruskal-Wallis H test results of fingerprint characteristic data set of source types in the small watershed of Nianyangou No.3 Dam

Soil sample types	Statistical indicators	Potential tracers													
		V (mg kg ⁻¹)	Cr (mg kg ⁻¹)	Mn (mg kg ⁻¹)	Co (mg kg ⁻¹)	Ni (mg kg ⁻¹)	Cu (mg kg ⁻¹)	Zn (mg kg ⁻¹)	As (mg kg ⁻¹)	Sb (mg kg ⁻¹)	TOC (mg kg ⁻¹)	¹³⁷ CS (Bq kg ⁻¹)	Clay (%)	Slit (%)	Sand (%)
Farmland	Min	52.09	82.04	410.89	10.19	33.75	15.86	55.69	12.42	5.72	1.24	0.09	0.16	9.99	69.93
	Mean	61.82	93.72	584.39	17.86	39.05	38.78	82.15	16.75	8.79	1.58	0.37	0.40	23.41	76.19
	Max	76.14	115.21	771.87	22.10	48.02	53.55	130.29	22.23	11.91	1.89	0.71	0.61	29.89	89.42
	CV	0.11	0.08	0.16	0.17	0.11	0.27	0.17	0.17	0.15	0.12	0.32	0.32	0.21	0.07
Grassland	Min	49.46	88.60	430.04	11.34	18.51	18.18	48.56	9.42	6.95	1.68	0.04	0.19	27.82	65.32
	Mean	57.55	100.88	602.87	17.60	25.95	40.06	81.58	13.43	8.02	2.02	0.83	0.34	31.76	67.90
	Max	67.19	120.04	968.04	21.95	35.60	56.75	110.65	21.41	9.91	2.33	2.19	0.49	34.19	71.79
	CV	0.10	0.10	0.22	0.14	0.16	0.20	0.18	0.18	0.11	0.08	0.33	0.21	0.07	0.03
Shrubland	Min	32.42	22.68	394.67	10.52	28.52	17.56	74.01	9.21	6.04	1.24	0.10	0.04	35.36	59.84
	Mean	50.08	39.72	585.37	19.19	29.53	32.94	99.13	12.53	11.16	1.83	0.66	0.25	37.72	62.03
	Max	65.14	49.97	915.05	25.71	31.33	56.21	129.63	16.77	18.13	2.62	2.76	0.35	39.86	64.29
	CV	0.17	0.21	0.22	0.17	0.03	0.24	0.14	0.15	0.23	0.15	0.31	0.28	0.04	0.03
Gully	Min	52.15	43.37	478.97	9.53	33.51	15.95	78.15	9.77	2.18	1.92	0.15	0.23	8.54	70.69
	Mean	67.65	51.54	677.08	16.46	39.51	34.84	108.47	16.27	17.64	2.43	1.60	0.53	23.74	75.73
	Max	75.17	59.58	994.25	26.25	48.86	55.41	139.01	22.26	29.31	3.18	5.43	1.10	28.79	90.36
	CV	0.09	0.10	0.16	0.26	0.12	0.23	0.14	0.20	0.37	0.13	0.31	0.22	0.26	0.08
Sediment core	Min	34.76	24.29	427.74	12.52	20.57	14.51	60.04	10.86	11.62	1.84	1.22	0.05	15.22	57.05
	Mean	52.23	64.24	597.44	16.81	29.94	23.54	84.63	14.50	16.93	2.38	2.81	0.27	24.58	75.15
	Max	75.04	117.64	856.13	23.38	44.56	50.44	114.85	21.86	24.29	3.27	4.43	0.70	42.31	84.63
	CV	0.15	0.38	0.21	0.18	0.25	0.35	0.22	0.17	0.21	0.13	0.32	0.53	0.28	0.09
Tracers conservative behavior ^{a,b}	P _{a,b}	P _{a,b}	P _{a,b}	P _{a,b}	P _{a,b}	P _{a,b}	P _{a,b}	P _{a,b}	P _{a,b}	P _a	P _a	P _a	P _{a,b}	P _{a,b}	
Statistical analysis	H value	13.304	28.117	2.992	1.8991	25.083	0.000**	0.594	0.000**	0.018*	10.067	7.5405	20.709	27.11	
	p value	0.004**	0.000**	0.393	0.393	0.594				0.057	0.064	0.000**		0.000**	

Notes: CV, coefficient of variation, **, extremely significant at a level of 0.01; *, significant at a level of 0.05; a, All sediment sample concentrations were within the range of the source sample values; b, The mean of sediment sample concentrations were within the range of the source sample values, and the coefficient of variation in sediment samples is smaller than that in source..

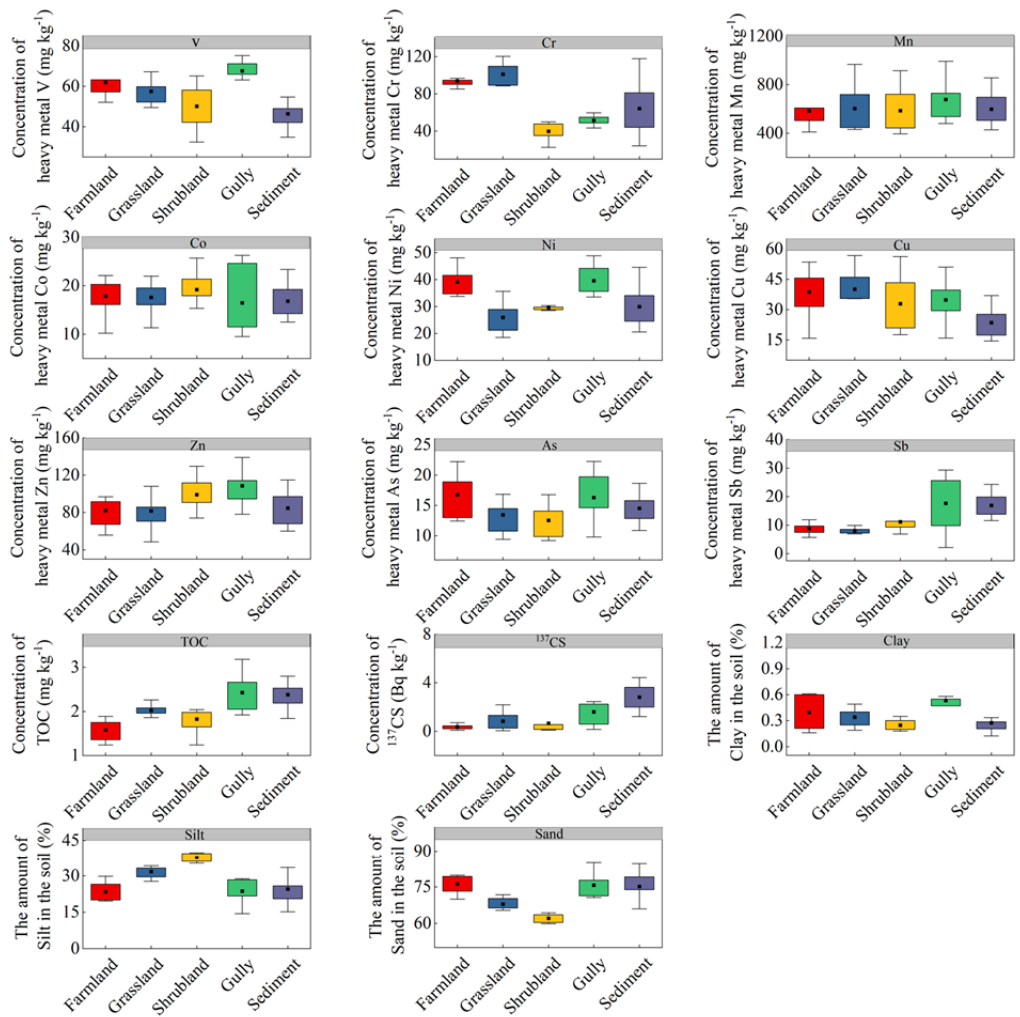


Fig. 8 Statistical map of geochemical properties of soils in different sampling areas. (The boxes indicate the interquartile range and the whiskers represent the maximum and minimum values. The square indicates the mean value.)

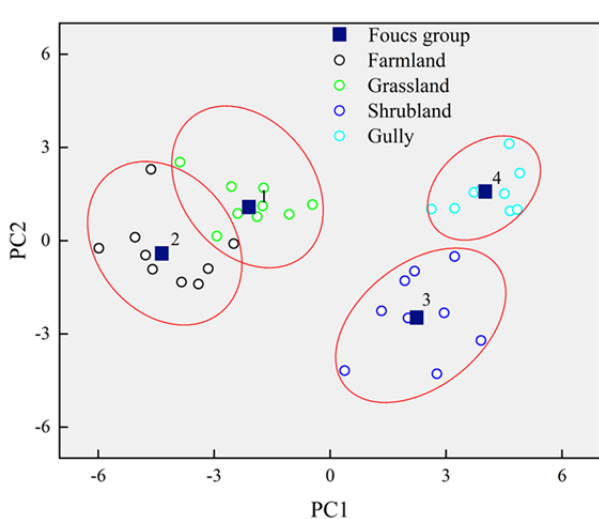


Fig. 9 Discriminant Function Analysis (DFA) of source samples.

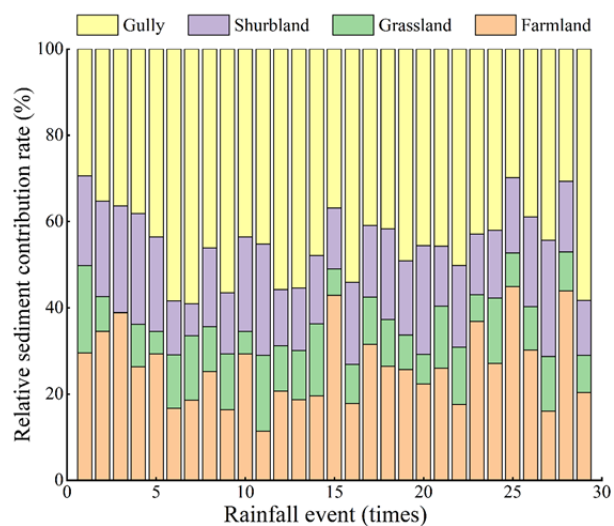
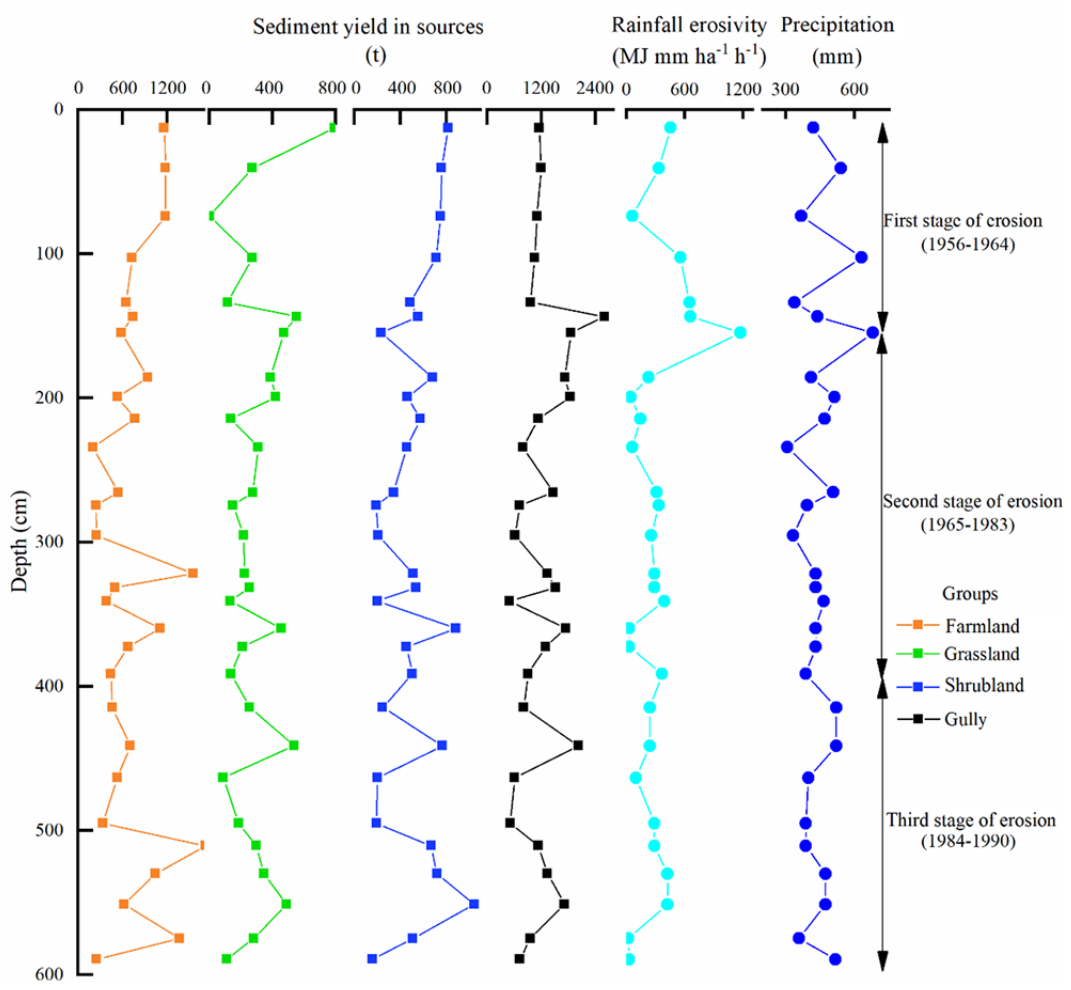


Fig. 10 Nianyangou No. 3 check dam sediment source contribution rate.

Table 2 Composite fingerprint tracers discrimination result. (The result of DFA showed that the total identification rate using these tracers was 97.2%).

Source category		Predicted group information				Total
		Farmland	Grassland	Shrubland	Gully	
Sample quantity	Farmland	8	1	0	0	9
	Grassland	0	9	0	0	9
	Shrubland	0	0	9	0	9
	Gully	0	0	0	9	9
Distinguish rate %	Farmland	88.9	11.1	0.0	0.0	100.0
	Grassland	0.0	100.0	0.0	0.0	100.0
	Shrubland	0.0	0.0	100.0	0.0	100.0
	Gully	0.0	0.0	0.0	100.0	100.0

**Fig.11** Sediment yield, annual rainfall and annual rainfall erosivity of each sediment source.

combination (TN, Fe, TP, and Ca) to determine the sediment sources in the Hujiawan catchment, in which the main source area corresponded to gullies ($44.1\% \pm 25.5\%$). By applying the best fingerprint combination (Xhf, TN, and ^{137}Cs) in the Huangjiagou Basin, Tian et al. (2019) calculated that $\sim 74.06\%$ of the sediment originated from weathered rocks. The findings of these studies are consistent with our findings. Gullies were the most eroded land use type

in the No. 3 check dam-controlled watershed, contributing 29.43%–58.43% of the sediment during the study period.

The main erosion source on the Loess Plateau is gully walls (Bai et al. 2022). The sediment yield from the gullies in this study was consistent with the variations in rainfall and rainfall erosivity. The gully walls are generally bare and covered by only sparse vegetation, as they are located under the slope where

sediment eroded from cropland, grassland, and shrubland are transported, thereby increasing the erosion energy. Zhao et al. (2017) reported that sediment was mainly sourced from gullies, followed by farmland, in the Gansu Province, China. Chen et al. (2016b) also found that gullies were the main sediment source (6.0.8%), followed by cropland (20.7%), forest land (11.3%), and grassland (7.2%). These findings are similar to those obtained herein. From 1956–1990, 80,350 t of sediment was intercepted in this small watershed, including 35,560 t of sediment from gullies, 21,500 t from farmland, 14,871 t from shrubland, and 8,410 t from grassland. This corresponds to an average erosion modulus of 12,710 t km⁻² from 1956–1990. The average soil erosion moduli of the gullies, farmland, shrubland, and grassland were 5,610, 3,390, 2,350, and 3,390 t km⁻², respectively.

4.2 Impacts of land use changes on erosion in source areas

Historical changes in sediment yield in source areas are related to land use changes; therefore, anthropogenic activity should also be considered to accurately assess historical soil erosion and predict future erosion events. Based on an analysis of existing data, the erosion environment was divided into three periods: (1) 1956–1965, (2) 1966–1983, and (3) 1984–1990. In general, the soil erosion modulus of the Nianyangou watershed decreased from 14,160 t km⁻² in the first period to 9,590 t km⁻² in the second period, then increased to 13,110 t km⁻² in the third period. Compared with the period 1956–1966, soil erosion in the watershed decreased by 32% from 1966 to 1983, but increased by 37% from 1984 to 1990 (Fig. 12).

These changes in erosion are related to local soil and water conservation policies. In the first period, China was in its “Great Leap Forward,” during which vegetation was destroyed and arable land increased, leading to a large erosion modulus in the basin. In the second period, active soil and water conservation policies were implemented and large areas of vegetation were restored, which greatly alleviated soil erosion within the basin and reduced soil erosion rates. In the third period, owing to the implementation of the “rural land contract responsibility system,” the arable land area increased and some vegetation was destroyed, resulting in more intense soil erosion (Zhang et al. 2020). The changes

in the erosion moduli of each source area are consistent with that of the total erosion modulus. The variability of changes in soil erosion during 1956–1990 in gullies was smaller than that on farmland. Soil erosion in gullies decreased by 26% from the periods of 1956–1965 to 1966–1986, but increased by 20% during 1984–1990. However, soil erosion on farmland decreased by 38% during 1956–1983 and increased by 58% during 1984–1990 (Fig. 11). As the primary sediment source area, gully not only represent the sediment generated by runoff, but also represent trench cutting, traceback, and collapse caused by gravity-driven erosion (Zhao et al. 2017); consequently, it did not vary widely. In contrast, arable land is located on slopes and is more vulnerable to anthropogenic activity. Arable land had a low soil erosion modulus when vegetation was restored (period 2), and a high soil erosion modulus when vegetation was destroyed (periods 1 and 3).

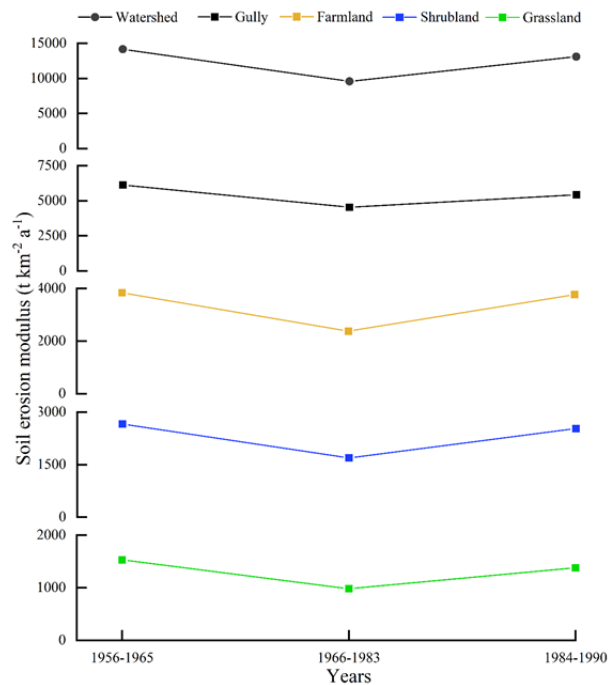


Fig.12 Variation of soil erosion modulus at different stages.

4.3 Land planning and management

According to Jiao et al. (2002), rational land use planning and check dam construction are the best measures for reducing soil erosion. Vegetation restoration is also a soil and water conservation method that can be applied on slopes (Shi et al. 2022), as vegetation can intercept runoff (i.e., by the

forest canopy and absorption by dead leaves) and improve the soil texture by increasing surface roughness and reducing the flow rate (Jin et al. 2021). Check dams are efficient channel-engineering measures that can both directly intercept runoff and sediment and change the underlying surface conditions in the basin (i.e., by raising the erosion base level and reducing gully drop) (Mandana et al. 2012). Therefore, soil and water losses can be controlled more efficiently through the rational application of soil and water conservation measures on slopes and the construction of check dams. When used simultaneously, these measures promote sustainable development on the Loess Plateau.

5 Conclusions

In this study, we used ^{137}Cs activity to identify 29 flood event layers (1956–1990) in sediment deposited at check dam No. 3 in the Nianyangou watershed in the central Loess Plateau. The layers can be divided into three erosion periods: 1956–1965, 1966–1983, and 1984–1990. The optimal combination of tracers (Cr, Ni, V, and TOC) selected in this study had a 97.2% source recognition ability. The contribution

rates of sediment from gullies, farmland, grassland, and shrubland were 44.89%, 26.38%, 10.49%, and 18.24%, respectively. Under natural rainfall conditions, the average sediment yields from gullies, farmland, grassland, and shrubland were 1,227, 751, 512, and 279 t, respectively. During all three erosion periods, the soil erosion rates in the source regions were influenced by rainfall and anthropogenic activity. Therefore, a combination of reasonable slope erosion mitigation measures and check dams may be a better way to reduce soil erosion in small watersheds on the Loess Plateau.

Acknowledgments

This work was supported by the Project of Creating Ordos National Sustainable Development Agenda Innovation Demonstration Zone (Grant 2022EEDSKJXM005), Natural Science Foundation of China (Grant 42077073), Natural Science Basic Research Plan in Shaanxi Province of China (2022KJXX-62), the Project of Shaanxi Coal and Chemical Industry Group Co., Ltd (2022SMHKJ-A-J-07-02, 2022SMHKJ-B-J-54), the Project of AnHui Water Resources Development Co., Ltd (KY-2021-13).

References

- Ahmady-Birgani H, Agahi E, Ahmadi SJ, et al. (2018) Sediment source fingerprinting of the Lake Urmia sand dunes. *Sci Rep* 8(1): 1-15. <https://doi.org/10.1038/s41598-017-18027-0>
- Bai L, Shi P, Yu K, et al. (2022) A new method to evaluate the accuracy of the sediment source mixing model. *Ecol Indic* 142: 109304. <https://doi.org/10.1016/j.ecolind.2022.109304>
- Boudreault M, Koiter AJ, Lobb DA, et al. (2019) Comparison of sampling designs for sediment source fingerprinting in an agricultural watershed in Atlantic Canada. *J Soils Sediments* 19(9). <https://doi.org/10.1007/s11368-019-02306-6>
- Cavalli M, Trevisani S, Comiti F, et al. (2013) Geomorphometric assessment of spatial sediment connectivity in small Alpine catchments. *Geomorphology* 188: 31-41. <https://doi.org/10.1016/j.geomorph.2012.05.007>
- Chen L, Wei W, Fu B, et al. (2007) Soil and water conservation on the Loess Plateau in China: review and perspective. *Prog Phys Geogr* 31(4): 389-403. <https://doi.org/10.1177/0309133307081290>
- Chen F, Zhang F, Fang N, et al. (2016a) Sediment source analysis using the fingerprinting method in a small catchment of the Loess Plateau, China. *J Soils Sediments* 16(5): 1655-1669. <https://doi.org/10.1007/s11368-015-1336-7>
- Chen F, Fang N, Shi Z (2016b) Using biomarkers as fingerprint properties to identify sediment sources in a small catchment. *Sci Total Environ* 557: 123-133. <https://doi.org/10.1016/j.scitotenv.2016.03.028>
- Chen F, Wang X, Li X, et al. (2019) Using the sediment fingerprinting method to identify the sediment sources in small catchments with similar geological conditions. *Agric Ecosyst Environ* 286: 106655. <https://doi.org/10.1016/j.agee.2019.106655>
- Cheng Y, Li P, Xu GC, et al. (2018) Effects of soil erosion and land use on spatial distribution of soil total phosphorus in a small watershed on the Loess Plateau, China. *Soil Tillage Res* 184: 142-152. <https://doi.org/10.1016/j.still.2018.07.011>
- Collins AL, Walling DE, Leeks GJL (1998) Use of composite fingerprints to determine the provenance of the contemporary suspended sediment load transported by rivers. *Earth Surf Process Landf* 23(1): 31-52. [https://doi.org/10.1002/\(sici\)1096-9837\(199801\)23:1<31::aid-esp816>3.0.co;2-z](https://doi.org/10.1002/(sici)1096-9837(199801)23:1<31::aid-esp816>3.0.co;2-z)
- Collins AL, Zhang Y, Walling DE, et al. (2010) Tracing sediment loss from eroding farm tracks using a geochemical fingerprinting procedure combining local and genetic algorithm optimisation. *Sci Total Environ* 408(22): 5461-5471. <https://doi.org/10.1016/j.scitotenv.2010.07.066>
- Evrard O, Durand R, Foucher A, et al. (2019) Using spectrophotometry to trace sediment source dynamics in coastal catchments draining the main Fukushima radioactive pollution plume (2011-2017). *J Soils Sediments* 19(9): 3290-3301. <https://doi.org/10.1007/s11368-019-02302-w>
- Feng XM, Fu BJ, Piao SL, et al. (2016) Revegetation in China's Loess Plateau is approaching sustainable water resource limits. *Nat Clim Chang* 6(11): 1019-1022. <https://doi.org/10.1038/nclimate3092>
- Fielding JJ, Croudace IW, Kemp AES, et al. (2020) Tracing lake pollution, eutrophication and partial recovery from the sediments of Windermere, UK, using geochemistry and sediment microfabrics. *Sci Total Environ* 722: 137745. <https://doi.org/10.1016/j.scitotenv.2020.137745>
- Gao J, Sang Y (2017) Identification and estimation of landslide-debris flow disaster risk in primary and middle school campuses in a mountainous area of Southwest China. *Int J*

- Disaster Risk Reduct 25: 60–71.
<https://doi.org/10.1016/j.jidrr.2017.07.012>
- Gaspar L, Blake WH, Smith HG, et al. (2019) Testing the sensitivity of a multivariate mixing model using geochemical fingerprints with artificial mixtures. *Geoderma* 337: 498–510.
<https://doi.org/10.1016/j.geoderma.2018.10.005>
- Gholami V, Sahour H, Hadian AMA (2021) Soil erosion modeling using erosion pins and artificial neural networks. *Catena* 196. <https://doi.org/10.1016/j.catena.2020.104902>
- Hu JF, Zhao GJ, Mu XM, et al. (2020) Effect of soil and water conservation measures on regime-based suspended sediment load during floods. *Sustain Cities Soc* 55: 102044.
<https://doi.org/10.1016/j.scs.2020.102044>
- Hu CH, Zhang XM (2020) Loess Plateau soil erosion governance and runoff-sediment variation of Yellow River. *Water Resources and Hydropower Engineering* 51(01):1-11. (In Chinese). <https://doi.org/10.13928/j.cnki.wrahe.2020.01.001>
- IUSS Working Group, W. R. B (2006) World reference base for soil resources 2006. World Soil Resources Reports no. 103. Food and Agriculture Organization (FAO), Rome.
- Jin F, Yang W, Fu J, et al. (2021) Effects of vegetation and climate on the changes of soil erosion in the Loess Plateau of China. *Sci Total Environ* 773: 145514.
<https://doi.org/10.1016/j.scitotenv.2021.145514>
- Jia X, Wang H, Wan H (2014) Sources and trace element geochemical characteristics of the coarse sediment in the Ningxia-Inner Mongolia reaches of the Yellow River. *Geosci J* 18(2): 181–192. <https://doi.org/10.1007/s12303-013-0052-9>
- Jiao JY, Li J, Wang WZ (2002) Erosion environment in the sediment-rich area on the Loess Plateau. *J Geogr Sci* 12(1): 49–57. <https://doi.org/10.1007/bf02837427>
- Jiang C, Zhang HY, Wang XC, et al. (2019) Challenging the land degradation in China's Loess Plateau: Benefits, limitations, sustainability, and adaptive strategies of soil and water conservation. *Ecol Eng* 127: 135–150.
<https://doi.org/10.1016/j.ecoleng.2018.11.018>
- Koiter AJ, Owens PN, Petticrew EL, et al. (2013) The behavioural characteristics of sediment properties and their implications for sediment fingerprinting as an approach for identifying sediment sources in river basins. *Earth Sci Rev* 125: 24–42. <https://doi.org/10.1016/j.earscirev.2013.05.009>
- Lance JC McIntyre SC, Naney JW, et al. (1986) Measuring sediment movement at low erosion rates using cesium - 137. *Soil Sci Soc Am J* 50(5): 1303–1309.
<https://doi.org/10.2136/sssaj1986.03615995005000050044x>
- Li XG, Wei X, Wei N (2016) Correlating check dam sedimentation and rainstorm characteristics on the Loess Plateau, China. *Geomorphology* 265: 84–97.
<https://doi.org/10.1016/j.geomorph.2016.04.017>
- Lin Y, Yao SB (2014) Impact of the Sloping Land Conversion Program on rural household income: An integrated estimation. *Land use policy* 40: 56–63.
<https://doi.org/10.1016/j.landusepol.2013.09.005>
- Mandana A, Md AMS, Fauziah A (2012) Effectiveness of check dam to control soil erosion in a tropical catchment (The Ulu Kinta Basin). *Catena* 97: 63–70.
<https://doi.org/10.1016/j.catena.2012.05.003>
- Mekonnen M (2021) Impacts of soil and water conservation practices after half of a generation age, northwest highlands of Ethiopia. *Soil Tillage Res* 205: 104755.
<https://doi.org/10.1016/j.still.2020.104755>
- Muñoz-Arcos E, Castillo A, Cuevas-Aedo A, et al. (2021) Sediment source apportionment following wildfire in an upland commercial forest catchment. *J Soils Sediments* 21(6): 2432–2449. <https://doi.org/10.1007/s11368-021-02943-w>
- Nistor CJ, Church M (2005) Suspended sediment transport regime in a debris-flow gully on Vancouver Island, British Columbia. *Hydrological Processes: Hydrol Process* 19(4): 861–885. <https://doi.org/10.1002/hyp.5549>
- Niu B, Qu J, Zhang XJ, et al. (2019) Quantifying provenance of reservoir sediment using multiple composite fingerprints in an arid region experiencing both wind and water erosion. *Geomorphology* 332: 112–121.
<https://doi.org/10.1016/j.geomorph.2019.02.011>
- Palazón L, Gaspar L, Latorre B, et al. (2015) Identifying sediment sources by applying a fingerprinting mixing model in a Pyrenean drainage catchment. *J Soils Sediments* 15(10): 2067–2085. <https://doi.org/10.1007/s11368-015-1175-6>
- Poesen JW, Hooke JM (1997) Erosion, flooding and channel management in Mediterranean environments of southern Europe. *Prog Phys Geogr* 21(2): 157–199.
<https://doi.org/10.1177/030913339702100201>
- Poesen J, Nachtergaele J, Verstraeten G, et al. (2003) Gully erosion and environmental change: importance and research needs. *Catena* 50(2–4): 91–133.
[https://doi.org/10.1016/S0341-8162\(02\)00143-1](https://doi.org/10.1016/S0341-8162(02)00143-1)
- Poesen J (2017) Soil erosion in the Anthropocene: Research needs. *Earth Surf Process Landf* 43(1): 64–84.
<https://doi.org/10.1002/esp.4250>
- Rutebuka J, Munyeshuli UA, Nkundwakazi O, et al. (2021) Effectiveness of terracing techniques for controlling soil erosion by water in Rwanda. *J Environ Manage* 277: 111369.
<https://doi.org/10.1016/j.jenvman.2020.111369>
- Shi P, Li P, Li ZB, et al. (2022) Effects of grass vegetation coverage and position on runoff and sediment yields on the slope of Loess Plateau, China. *Agric Water Manag* 259: 107231. <https://doi.org/10.1016/j.agwat.2021.107231>
- Shi P, Li Z, Li P, et al. (2021) Trade-offs among ecosystem services after vegetation restoration in China's loess plateau. *Nat Resour Res* 30: 2703–2713.
<https://doi.org/10.1007/s11053-021-09841-5>
- Silva-Filho EV, Sanders CJ, Bernat M, et al. (2011) Origin of rare earth element anomalies in mangrove sediments, Sepetiba Bay, SE Brazil: used as geochemical tracers of sediment sources. *Environ Earth Sci* 64(5): 1257–1267.
<https://doi.org/10.1007/s12665-011-0942-y>
- Slimane AB, Raclot D, Evrard O, et al. (2013) Fingerprinting sediment sources in the outlet reservoir of a hilly cultivated catchment in Tunisia. *J Soils Sediments* 13(4): 801–815.
<https://doi.org/10.1007/s11368-012-0642-6>
- Tian P, An ZF, Zhao GJ, et al. (2019) Assessing sediment yield and sources using fingerprinting method in a representative catchment of the Loess Plateau, China. *Environ Earth Sci* 78(8): 261–263. <https://doi.org/10.1007/s12665-019-8240-1>
- Walling DE, Peart MR, Oldfield F, et al. (1979) Suspended sediment sources identified by magnetic measurements. *Nature* 281(5727): 110–113.
<https://doi.org/10.1038/281110ao>
- Walling DE (2005) Tracing suspended sediment sources in catchments and river systems. *Sci Total Environ* 344(1–3): 159–184. <https://doi.org/10.1016/j.scitotenv.2005.02.011>
- Wang Z, Chen Z, Yu S, et al. (2021) Erosion-control mechanism of sediment check dams on the Loess Plateau. *Int J Sediment Res* 36(5): 668–677.
<https://doi.org/10.1016/j.ijsrc.2021.02.002>
- Wen X, Deng X (2020) Current soil erosion assessment in the Loess Plateau of China: A mini-review. *J Clean Prod* 276: 123091. <https://doi.org/10.1016/j.jclepro.2020.123091>
- Wen X, Zhen L (2020) Soil erosion control practices in the Chinese Loess Plateau: A systematic review. *Environ Dev* 34: 100493. <https://doi.org/10.1016/j.envdev.2019.100493>
- Xiao J, Lv G, Chai N, et al. (2022) Hydrochemistry and source apportionment of boron, sulfate, and nitrate in the Fen River, a typical loess covered area in the eastern Chinese Loess Plateau. *Environ Res* 206: 112570.
<https://doi.org/10.1016/j.enres.2021.112570>
- Xu G, Cheng S, Li P, et al. (2018) Soil total nitrogen sources on dammed farmland under the condition of ecological construction in a small watershed on the Loess Plateau, China. *Ecol Eng* 121: 19–25.
<https://doi.org/10.1016/j.ecoleng.2017.09.005>
- Zhang J, Yang M, Zhang F, et al. (2017) Fingerprinting sediment sources after an extreme rainstorm event in a small catchment on the Loess Plateau, China. *Land Degrad Dev* 28(8): 2527–2539. <https://doi.org/10.1002/ldr.2803>
- Zhang Y, Zhang X, Bi Z, et al. (2020) The impact of land use changes and erosion process on heavy metal distribution in the hilly area of the Loess Plateau, China. *Sci Total Environ* 718: 137305. <https://doi.org/10.1016/j.scitotenv.2020.137305>
- Zhao T, Yang M, Walling DE, et al. (2017a) Using check dam deposits to investigate recent changes in sediment yield in the Loess Plateau, China. *Global Planet Change* 152: 88–98.
<https://doi.org/10.1016/j.gloplacha.2017.03.003>
- Zhao G, Mu X, Han M, et al. (2017b) Sediment yield and sources in dam-controlled watersheds on the northern Loess Plateau. *Catena* 149: 110–119. <https://doi.org/10.1016/j.catena.2016.09.010>
- Zhou H, Chang W, Zhang L (2016) Sediment sources in a small agricultural catchment: A composite fingerprinting approach based on the selection of potential sources. *Geomorphology* 266: 11–19. <https://doi.org/10.1016/j.geomorph.2016.05.007>